THE JOURNAL OF PHYSICAL CHEMISTRY Letters

Letter

pubs.acs.org/JPCL

A VUV Photoionization and Ab Initio Determination of the Ionization Energy of a Gas-Phase Sugar (Deoxyribose)

Debashree Ghosh,[†] Amir Golan,[‡] Lynelle K. Takahashi,[‡,§] Anna I. Krylov,[†] and Musahid Ahmed*[,‡]

[†]Department of Chemistry, University of Southern California, Los Angeles, California 90089-0482, United States

[‡]Chemical Sciences Division, Lawrence Berkeley National Laboratory, Berkeley, California 94720, United States

[§]Department of Chemistry, University of California at Berkeley, Berkeley, California 94720, United States

Supporting Information

ABSTRACT: The ionization energy of gas-phase deoxyribose was determined using tunable vacuum ultraviolet synchrotron radiation coupled to an effusive thermal source. Adiabatic and vertical ionization energies of the ground and first four excited states of α-pyranose, the structure that dominates in the gas phase, were calculated using high-level electronic structure methods. An appearance energy of 9.1($\pm$0.05) eV was recorded, which agrees reasonably well with a theoretical value of 8.8 eV for the adiabatic ionization energy. A clear picture of the dissociative photoionization dynamics of deoxyribose emerges from the fragmentation pattern recorded using mass spectrometry and from ab initio molecular dynamics calculations. The experimental threshold 9.4 ($\pm$0.05) eV for neutral water elimination upon ionization is captured well in the calculations, and qualitative insights are provided by molecular orbital analysis and molecular dynamics snapshots along the reaction coordinate.

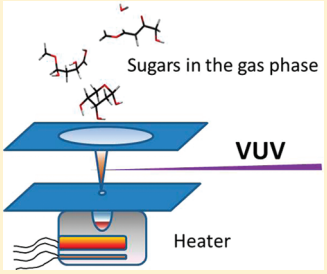

SECTION: Dynamics, Clusters, Excited States

Sugars, together with phosphates, constitute the scaffold on which nucleic acids build up DNA's structure. 2-Deoxy-D-ribose, the "D" in DNA, exists predominantly in the pyranose form in the aqueous phase, and it is believed to maintain this structure in the gas phase too.[1] The interaction of energy (X-rays, electrons, particles, vacuum ultraviolet (VUV) photons) with DNA has been studied in detail over a number of years, yet some basic questions regarding the electronic structure of the building blocks of DNA remain unanswered.[2,3] For example, a question such as "what is the ionization energy of deoxyribose?" does not generate a number with much certainty. There is one report in the literature of a 10.5 eV ionization energy measured using electron ionization,[4] and a few theoretical calculations present numbers around this value.[5−8] This is a surprisingly high value for a molecule that contains oxygen in a ring structure. Similar molecules such as tetrahydrofuran have much lower ionization energies, and there is near perfect agreement between theory and experiment for that molecule.[9,10] There have also been a number of experimental and theoretical[11,12] studies on the fragmentation of deoxyribose molecules from energetic radiation. However, these have often relied on an ionization energy of 10.5 eV or higher for the parent molecule to explain the experimental results.[4−6,13] The inability to generate an experimental ionization energy for sugars such as deoxyribose stems from the difficulty to prepare intact molecules in the gas phase for subsequent interrogation by ionizing radiation.

In this study we employ a gentle thermal desorption method coupled to tunable VUV photoionization to measure an experimental ionization energy for deoxyribose and to study its fragmentation mechanisms. We compare the experimental measurements with electronic structure calculations of vertical and adiabatic ionization energies (VIEs and AIEs). Ab initio molecular dynamics (AIMD) simulations are used to understand different fragmentation channels obtained via dissociative photoionization. The results and techniques described here will aid in the general understanding of the electronic structure of sugars, a topic of much discussion recently since biofuels are being seen as 21st century transportation fuels.[14] There is great interest in understanding the thermal and photoionization dynamics of molecules such as cellulose, levoglucosan, glucose, and cellobiose, among other molecules.[15,16] Our group has started a systematic program to study the photoionization and desorption dynamics of biomolecules,[17,18] sugars, and other lignocellulosic[19] material using a variety of experimental and theoretical methods, and here, to the best of our knowledge, we present the first experimental photoionization energy measurement for deoxyribose and an accurate calculated value of its ionization energy.

The relative energies of the pyranose, furanose, and ribose forms of 2-deoxy-D-ribose (Figure 1) are given in Table 1 (the estimated uncertainty of the method employed is ~2.5 kcal/mol.[20]). The pyranose form is 7.9 kcal/mol lower than furanose in the gas phase. Thus, although furanose is the most common form in DNA, pyranose is the most abundant form in the gas phase and solution. The pyranose structures have two isomers (α and β) depending on the OH group position in C_1. The α

Received: October 31, 2011
Accepted: December 14, 2011
Published: December 14, 2011

   dx.doi.org/10.1021/jz201446r | J. Phys. Chem.Lett. 2012, 3, 97−101

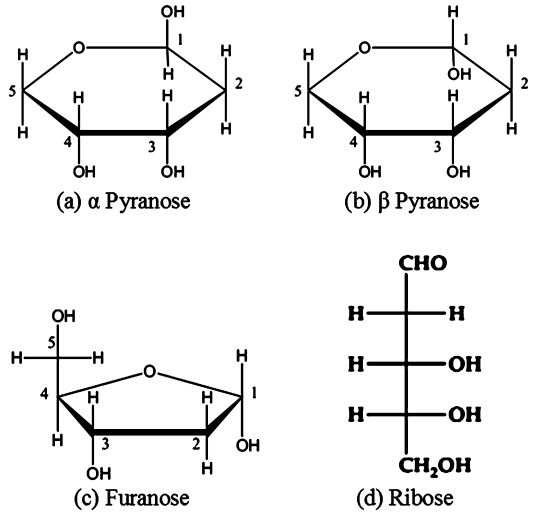

Figure 1. Structures of furanose, α and β pyranose, and ribose forms of 2-deoxy-D-ribose.

Table 1. Relative Stability of the Gas-Phase Furanose, Pyranose, and Ribose Forms Computed by DFT/ωB97x/cc-pVTZ

species	rel. energy in kcal/mol	Boltzmann population %
furanose	7.9	0.1
α-pyranose	0.0	99.0
β-pyranose	5.6	0.8
ribose	10.3	0.01

structure has the OH group pointing down in the Hayworth (or Fischer) diagram and β structure has the OH group pointing up. The α structure is more stable by 5.6 kcal/mol than the β form and the open-chain (ribose) structure is the least stable (10.3 kcal/mol higher than α pyranose). A Boltzmann population analysis predicts that 99% of the deoxyribose is in the α-pyranose form.

Figure 2 shows a mass spectrum of deoxyribose photoionized at 10.5 eV. As one can see, the fragmentation is quite extensive

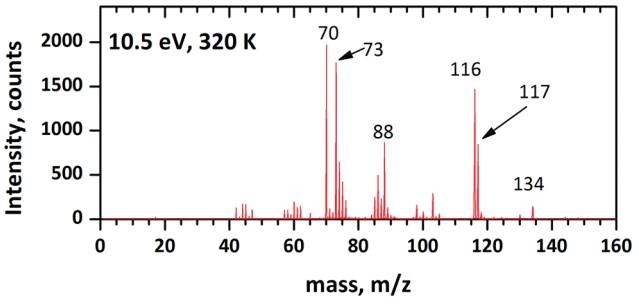

Figure 2. Experimental mass spectrum of deoxyribose gas-phase molecules recorded using an effusive source maintained at 320 K and photoionized at 10.5 eV.

at this energy. The parent peak is discernible at m/z 134, while major peaks are observed at m/z 70, 73, 88, 116, and 117. The photoionization efficiency curves (PIE) for all the major fragments are shown in the SM. At lower ionization energies, the parent peak (m/z = 134) is dominant, followed by m/z = 116. The low population in the parent ion relatively close to threshold is reminiscent of what occurs in SF_6, where upon ionization, even at threshold, it dissociated to SF_5^+.[21] Mass fragments at 70, 73, and 116 amu dominate the spectrum. A new peak at 117 amu is also prominent. The m/z 116 features arise from elimination of H_2O.

Extensive fragmentation has been noted from deoxyribose upon electron ionization,[4] VUV ionization,[13] and particle bombardment.[6] The mass fragments at m/z = 70, 73, 88, 103, 116, and 117 amu have been observed under these conditions, but very little or no parent cation (m/z = 134) has been seen in these earlier experiments. In a previous VUV photoionization study of deoxyribose,[13] the parent mass at m/z = 134 was not detected, and there was extensive fragmentation, similar to a 70 eV electron ionization mass spectrum. Recently Shin et al.[5] laser-desorbed a deoxyribose/R6G mixture and, using 26.44 eV laser photons for ionization, saw extensive fragmentation similar to that seen in earlier work using electron impact and VUV ionization and no evidence for the parent cation. In our case, thermal desorption at lower temperatures (300−325 K) should give rise to less decomposition and ionization at threshold and allows for detection of the parent cation albeit with small signal. The fragmentation is less extensive at lower ionization energies, e.g., using 9.5 eV photons, the parent peak is dominant, and is followed by m/z = 116 (water elimination), which is identified as a major fragmentation channel.

The computed (ωB97x/cc-pVTZ) gas-phase ionization energies (VIE and AIE) of the 2-deoxy-D-ribose are given in Table. 2. The IEs for the lowest isomer, α-pyranose, were

Table 2. VIEs and AIEs of 2-Deoxy-D-ribose Isomers (in eV) Computed by ωB97x/cc-pVTZ

species	VIE	AIE w/o ZPE[a]	AIE w/ZPE[a]	Koopmans VIE
furanose	10.06	9.05	8.98	10.15
α-pyranose	9.60	8.86	8.81	9.71
β-pyranose	9.63	8.74	8.70	9.71
ribose	9.91	9.03	8.99	9.93

[a]Zero point energy.

benchmarked against equation-of-motion coupled-cluster with singles and doubles (EOM-IP-CCSD) using cc-pVTZ, and the differences were less than 0.05 eV. Previous studies of IEs using EOM-IP-CCSD/cc-pVTZ have shown average errors <0.1 eV.[22−24] Thus, the estimated uncertainty in the calculated IEs is 0.1 eV.

Both the α and β forms of pyranose have very similar IEs, while the furanose and ribose forms have higher IEs. The AIE with ZPE for α-pyranose is calculated to be 8.81 eV (8.86 without zero point energy (ZPE)) and agrees reasonably well with our measured appearance energy of 9.1 eV shown in the PIE curve for the parent mass in Figure 3A. The discrepancy of 0.2 eV between theoretical and experimental values is likely to be due to unfavorable Franck−Condon factors (FCFs); similar magnitude difference between 00 transitions and the computed apparent PIE onset has been observed in a previous study of thymine-water clusters.[22] The PIE shown in Figure 3A rises gradually up to 9.55 eV, plateaus for 0.1 eV, and then continues rising up to 11.00 eV. Our calculated VIE of 9.60 eV suggests poor FCFs for ionization. Experimentally, this manifests as the broad onset in the PIE shape as opposed to a sharp step function. Attempts were made to calculate the FCFs and to generate a photoelectron spectrum using the ezSpectrum code[25] (based on double-harmonic approximation), which has been successfully applied to compare experimental and theoretical results for thymine, thymine clustered with water,

dx.doi.org/10.1021/jz201446r | J. Phys. Chem.Lett. 2012, 3, 97−101

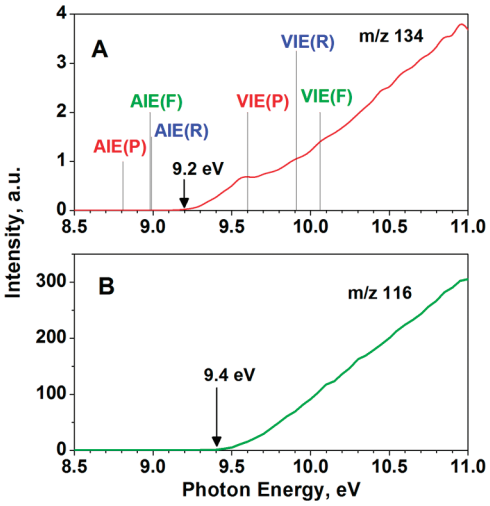

Figure 3. (A) An experimental PIE curve for deoxyribose recorded with a step size of 50 meV. The vertical lines denote calculated AIEs and VIEs of the furanose (F), pyranose (P), and ribose (R) forms of deoxyribose, respectively. (B) A PIE curve for m/z 116. The experimental appearance energies are indicated by arrows. Errors in the experimental determination are ± 0.05 eV.

and other nucleobases.[23,24] Contrarily to these previous studies, the shape of the computed PIE curve did not agree with the experimental one, most likely due to significant ionization-induced distortions and anharmonic effects one would expect for such a nonrigid molecule as deoxyribose.

The molecular orbitals (MOs) giving rise to the first 4 lowest-energy ionized states are shown in Figure 4. These

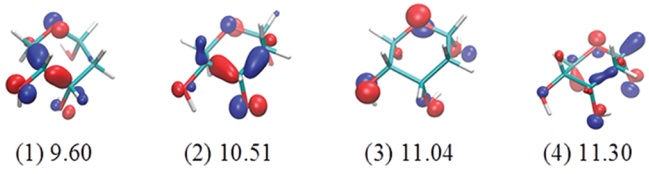

Figure 4. MOs and VIEs (in eV) for the lowest four ionized states of the α pyranose form of deoxyribose. The EOM-IP-CCSD/cc-pVTZ amplitudes for these orbitals are 0.95, 0.92, 0.92, and 0.93, respectively, revealing dominant Koopmans character of the ionized states.

computed EOM-IP-CCSD/cc-pVTZ ionization energies (VIEs are 9.60, 10.51, 11.04, 11.30 eV) suggest that the second ionization onward will contribute to the rise of signal in the experimental curve only beyond 10.5 eV. Thus, these states will not be discussed further. Future photoelectron or ion-electron coincidence experiments should allow these ionizations to be followed experimentally. The MO from which the first ionization occurs has significant electron density in the oxygen lone pairs, lp(O), and on the bonding σ orbital between C_4–C_5 (and, to a lesser degree, between C_3–C_4). Thus, removing the electron from this orbital results in weakening of the C_4–C_5 bond in the cationic species (1.84 Å versus 1.53 Å in the neutral). The distribution of spin-density (included in the Supporting Information) confirms the conclusion that the hole is delocalized almost equally over oxygen, C_4 and C_5. Further details of the structural changes of the cationic species are given in the Supporting Information.

While the FC calculations (see Supporting Information) were not successful in reproducing the experimental PIE curve, they do aid in understanding the fragmentation mechanisms. The examination of the simulated photoelectron spectrum shown in Figure S5 of the Supporting Information reveals that the ν_2, ν_6, ν_8, ν_{11}, ν_{15}, ν_{21}, ν_{23}, ν_{35} modes are FC active. The largest displacement is along the ν_{11} mode (CH bending around C_2 and C_3, and twist along the C_5O bond in the ring); the overtones or combination bands of ν_{11} give rise to the dominant progression. The other important normal modes are ν_0, ν_6, ν_{24}, and ν_{50}. ν_0 consists of CO bending at the OH groups of C_1 and C_4, and CH bending at C_5. ν_6 involves OH bending at C_3 and CH bending at C_2 and C_5. ν_{24} is a combination of CH bending at C_2, C_3, and C_4. ν_5 consists of CO bending and OH stretching at C_3.

To gain insight into the mechanism of the dissociative photoionization, we carried out AIMD calculations with B3LYP/6-31+G(d,p) at T = 300 K starting from initial structures that are slightly displaced along the most FC-active modes described above. We notice that significant fragmentation occurs within 4 ps, and that a large fraction of the cations decay via the water elimination channel (m/z = 116), which is the dominant fragmentation channel at low ionization energy (e.g., at 9.5 eV) as can be seen by looking at the PIE curves for all species (Supporting Information). At this time scale, the AIMD predicts that the major fragmentation channels are those leading to neutral H_2O (m/z = 116) and CH_2O (m/z = 104, 86, 60 and 44, see Supporting Information for chemical structures). m/z = 104 is produced by CH_2O elimination, while the m/z = 86, 60, and 44 fragments are formed by secondary fragmentation following CH_2O elimination. Another channel that we observed is the elimination of CH_3O (m/z = 103). Experimentally, apart from m/z = 104, all the other fragments have been observed. However, strong signals observed at m/z = 70 and 73 are not reproduced by the simulations. Previous experiments[13] show the presence of m/z = 104, 86, 60, and 44 (which are predicted by AIMD). Since only 50 trajectories were run, it is unrealistic to expect to observe all possible fragmentation channels in these limited simulations. Moreover, we did not perform an exhaustive investigation of secondary fragmentation channels.

Further analysis of AIMD trajectories sheds light on the mechanism of the major fragmentation channel of H_2O elimination. The trajectories reveal that most of the fragmentation events start with the C_4–C_5 bond breaking, in accordance with our expectations based on the analysis of the MO shape and FCFs. Since the C_4–C_5 bond is significantly weakened in the cation (as evidenced by its elongated bond length of 1.84 Å), it is most likely to break causing the cyclic structure to unfurl. This allows the OH groups on C_3 and C_1 to come close to each other, which is promptly followed by water elimination. The reaction progress can be monitored by observing the time evolution of the C_4–C_5 bond length as well as the OH bond lengths (see Supporting Information). To understand the nature of the reaction barrier, we took snapshots from the MD trajectories and performed constrained optimization (such calculations yield energy profile along an approximate reaction coordinate). During the ring-opening part of the trajectory, the reaction coordinate can be approximated by the C_4–C_5 distance (which is, therefore, frozen in optimizations), whereas the second part (water elimination facilitated by the OH groups on C_3 and C_1 approaching each other) is represented by the O–H bond length of the C_1 carbon.

dx.doi.org/10.1021/jz201446r | J. Phys. Chem.Lett. 2012, 3, 97–101

Figure 5 shows the free energy change from the vertically ionized pyranose (the reactant), to the transition state (TS,

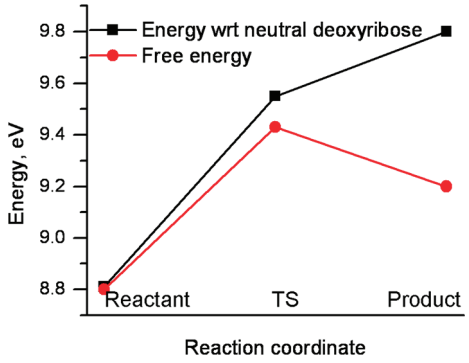

Figure 5. The free energy along the reaction coordinate of the constrained optimized structures taken from AIMD snapshots. Entropy contribution (wrt stands for with respect to) was evaluated within the RRHO approximation.

which can be described as an open-chain structure), to the products, calculated from the energy of the constrained optimized structures and the entropy within the rigid-rotor-harmonic-oscillator (RRHO) approximation. The energy along the reaction coordinate increases, since it is dominated by bond-breaking (C_4–C_5, C_3–O, C_1O–H bonds break, and one OH bond is formed), which is endothermic. However, the entropy increase leads to negative free energy change. The computed approximate minimum energy path suggests that the rate-determining step is the bond breaking and subsequent opening up of the ring (~9.4 ± 0.5 eV barrier), which is in excellent agreement with the experimental onset for the water elimination channel (Figure 3B). These approximate calculations of the minimum energy path were validated by computing a fully optimized TS, which yielded a very similar structure and a ~9.8 eV barrier. Supporting Information shows the structure of the reactant, product, and the TS, as well as a movie of the water elimination channel.

In sum, water elimination from the ionized pyranose proceeds through the following steps: (i) C_4–C_5 bond breaking, (ii) unfurling of the ring and the OH groups of C_1 and C_3 approaching each other, (iii) C_1–O and C_3O–H bond elongation and C_1O–HOC_3 bond formation, and (iv) water elimination by combining the OH group from C_1 and H atom from C_3–OH. The rate limiting step is the unfurling of the ring and the proper orientation of the OH groups to initiate water elimination.

To conclude, we have measured an experimental AIE of 9.1 eV for deoxyribose in the pyranose form in the gas phase, and this value agrees reasonably well with a theoretical estimate of 8.8 eV. Electronic structure and AIMD calculations provide insight into the water elimination pathway upon deoxyribose dissociative photoionization, and the calculated 9.8 eV barrier agrees well with experimental observations. This combined experimental and theoretical approach in studying the dissociative photoionization of a model sugar will find application in studying biomass decomposition where VUV photoionization mass spectrometry is being proposed as a tool for chemical analysis. The calculations will aid the design of future experiments to probe the dynamics of the dissociative photoionization using ion-electron coincidence or ultrafast pump probe experiments with VUV photons.

EXPERIMENTAL AND COMPUTATIONAL

The experiments were performed at the Chemical Dynamics Beamline at the Advanced Light Source (Supporting Information). Deoxyribose was gently desorbed via thermal heating and subsequently ionized by tunable VUV synchrotron radiation and extracted into a reflectron time-of-flight (TOF) mass spectrometer. A TOF mass spectrum is recorded at photon energies between 8.5 and 11.0 eV, with 50 meV resolution, and PIE curves are extracted from these data sets. The optimized geometries of the pyranose and furanose form of 2-deoxy-D-ribose were calculated by density functional theory (DFT) with the ωB97x functional[20] and the cc-pVTZ basis set[26] to identify the most stable structure in the gas phase. The optimized structures of the cationic species were calculated at the same level of theory. The VIEs and AIEs were computed with DFT as well as EOM-IP-CCSD[27−32] using the same basis set. The fragmentation dynamics of the cationic species was analyzed using AIMD simulations with the B3LYP functional[33,34] and the 6-31+G(d,p) basis set using 2 fs time step and T = 300 K. The water elimination channel (which was found experimentally to be one of the dominant fragmentation channels) was further studied by optimizing the structures with constraints (at the ωB97x/cc-pVTZ level) along the reaction path obtained from AIMD snapshots. The entropic effects were calculated within the RRHO approximation to estimate the barrier for the water elimination process. All calculations were performed using the Q-Chem electronic structure program.[35]

ASSOCIATED CONTENT

Supporting Information

Theoretical description of the structure and character of the deoxyribose cation, calculation of the water elimination channel for fragmentation, movie of the water elimination channel, calculated photoelectron spectrum, experimental PIE curves of major fragments, and optimized geometries of deoxyribose. This material is available free of charge via the Internet at http://pubs.acs.org

AUTHOR INFORMATION

Corresponding Author

*Mailing address: Lawrence Berkeley National Laboratory, 1 Cyclotron Road, MS 6R-2100, Berkeley, CA 94720, USA. Phone: (510) 486-6355; fax: (510) 486-5311; e-mail: MAhmed@lbl.gov.

ACKNOWLEDGMENTS

This work is supported by the Office of Science, Office of Basic Energy Sciences, of the U.S. Department of Energy under Contract No. DE-AC02-05CH11231, through the Chemical Sciences Division (A.G., L.K.T., M.A., and the Advanced Light Source), and DE-FG02-05ER15685 (A.K.). The calculations were conducted using resources of the iOpenShell Center for Computational Studies of Electronic Structure and Spectroscopy of Open-Shell and Electronically Excited Species (iopenshell.usc.edu) supported by the National Science Foundation through the CRIF:CRF CHE-0625419+0624602+0625237.

REFERENCES

(1) Guler, L. P.; Yu, Y. Q.; Kenttamaa, H. I. An Experimental and Computational Study of the Gas-Phase Structures of Five-Carbon Monosaccharides. *J. Phys. Chem. A* **2002**, *106*, 6754−6764.

(2) Shukla, M. K.; Leszczynski, J. In *Radiation Induced Molecular Phenomena in Nucleic Acids*; Shukla, M. K., Leszczynski, J., Eds.; Springer: New York, 2008; p 1.
(3) Baccarelli, I.; Gianturco, F. A.; Scifoni, E.; Solov'yov, A. V.; Surdutovich, E. Molecular Level Assessments of Radiation Biodamage. *Eur. Phys. J. D* **2010**, *60*, 1−10.
(4) Ptasinska, S.; Denifl, S.; Scheier, P.; Mark, T. D. Inelastic Electron Interaction (Attachment/Ionization) with Deoxyribose. *J. Chem. Phys.* **2004**, *120*, 8505−8511.
(5) Shin, J.-W.; Dong, F.; Grisham, M. E.; Rocca, J. J.; Bernstein, E. R. Extreme Ultraviolet Photoionization of Aldoses and Ketoses. *Chem. Phys. Lett.* **2011**, *506*, 161−166.
(6) Alvarado, F.; Bernard, J.; Li, B.; Bredy, R.; Chen, L.; Hoekstra, R.; Martin, S.; Schlatholter, T. Precise Determination of 2-Deoxy-D-ribose Internal Energies after keV Proton Collisions. *ChemPhysChem* **2008**, *9*, 1254−1258.
(7) Colson, A. O.; Besler, B.; Sevilla, M. D. Ab Initio Molecular Orbital Calculations on DNA Radical Ions 0.3. Ionization Potentials and Ionization Sites in Components of the DNA Sugar Phosphate Backbone. *J. Phys. Chem.* **1993**, *97*, 8092−8097.
(8) Slavicek, P.; Winter, B.; Faubel, M.; Bradforth, S. E.; Jungwirth, P. Ionization Energies of Aqueous Nucleic Acids: Photoelectron Spectroscopy of Pyrimidine Nucleosides and ab Initio Calculations. *J. Am. Chem. Soc.* **2009**, *131*, 6460−6467.
(9) Dampc, M.; Mielewska, B.; Siggel-King, M. R. F.; King, G. C.; Zubek, M. Threshold Photoelectron Spectra of Tetrahydrofuran over the Energy Range 9−29 eV. *Chem. Phys.* **2009**, *359*, 77−81.
(10) Milosavljevic, A. R.; Kocisek, J.; Papp, P.; Kubala, D.; Marinkovic, B. P.; Mach, P.; Urban, J.; Matejcik, S. Electron Impact Ionization of Furanose Alcohols. *J. Chem. Phys.* **2010**, *132*, 104308−104311.
(11) Baccarelli, I.; Gianturco, F. A.; Grandi, A.; Sanna, N. Metastable Anion Fragmentations after Resonant Attachment: Deoxyribosic Structures from Quantum Electron Dynamics. *Int. J. Quantum Chem.* **2008**, *108*, 1878−1887.
(12) Baccarelli, I.; Gianturco, F. A.; Grandi, A.; Sanna, N.; Lucchese, R. R.; Bald, I.; Kopyra, J.; Illenberger, E. Selective Bond Breaking in β-D-Ribose by Gas-Phase Electron Attachment around 8 eV. *J. Am. Chem. Soc.* **2007**, *129*, 6269−6277.
(13) Vall-Ilosera, G.; Huels, M. A.; Coreno, M.; Kivimaki, A.; Jakubowska, K.; Stankiewicz, M.; Rachlew, E. Photofragmentation of 2-Deoxy-D-ribose Molecules in the Gas Phase. *ChemPhysChem* **2008**, *9*, 1020−1029.
(14) Huber, G. W.; Iborra, S.; Corma, A. Synthesis of Transportation Fuels from Biomass: Chemistry, Catalysts, and Engineering. *Chem. Rev.* **2006**, *106*, 4044−4098.
(15) Lin, Y. C.; Cho, J.; Tompsett, G. A.; Westmoreland, P. R.; Huber, G. W. Kinetics and Mechanism of Cellulose Pyrolysis. *J. Phys. Chem. C* **2009**, *113*, 20097−20107.
(16) Bahng, M. K.; Mukarakate, C.; Robichaud, D. J.; Nimlos, M. R. Current Technologies for Analysis of Biomass Thermochemical Processing: A Review. *Anal. Chim. Acta* **2009**, *651*, 117−138.
(17) Kostko, O.; Takahashi, L. K.; Ahmed, M. Desorption Dynamics, Internal Energies, and Imaging of Organic Molecules from Surfaces with Laser Desorption and Vacuum Ultraviolet (VUV) Photoionization. *Chem. Asian J.* **2011**, *6*, 3066−3076.
(18) Zhou, J.; Takahashi, L. K.; Wilson, K. R.; Leone, S. R.; Ahmed, M. Internal Energies of Ion-Sputtered Neutral Tryptophan and Thymine Molecules Determined by Vacuum Ultraviolet Photoionization. *Anal. Chem.* **2010**, *82*, 3905−3913.
(19) Takahashi, L. K.; Zhou, J.; Kostko, O.; Golan, A.; Leone, S. R.; Ahmed, M. Vacuum-Ultraviolet Photoionization and Mass Spectrometric Characterization of Lignin Monomers Coniferyl and Sinapyl Alcohols. *J. Phys. Chem. A* **2011**, *115*, 3279−3290.
(20) Chai, J. D.; Head-Gordon, M. Long-Range Corrected Hybrid Density Functionals with Damped Atom−Atom Dispersion Corrections. *Phys. Chem. Chem. Phys.* **2008**, *10*, 6615−6620.
(21) Peterka, D. S.; Ahmed, M.; Ng, C. Y.; Suits, A. G. Dissociative Photoionization Dynamics of SF_6 by Ion Imaging with Synchrotron Undulator Radiation. *Chem. Phys. Lett.* **1999**, *312*, 108−114.
(22) Ghosh, D.; Isayev, O.; Slipchenko, L. V.; Krylov, A. I. Effect of Solvation on the Vertical Ionization Energy of Thymine: From Microhydration to Bulk. *J. Phys. Chem. A* **2011**, *115*, 6028−6038.
(23) Khistyaev, K.; Bravaya, K. B.; Kamarchik, E.; Kostko, O.; Ahmed, M.; Krylov, A. I. The Effect of Microhydration on Ionization Energies of Thymine. *Faraday Discuss.* **2011**, *150*, 313−330.
(24) Bravaya, K. B.; Kostko, O.; Dolgikh, S.; Landau, A.; Ahmed, M.; Krylov, A. I. Electronic Structure and Spectroscopy of Nucleic Acid Bases: Ionization Energies, Ionization-Induced Structural Changes, and Photoelectron Spectra. *J. Phys. Chem. A* **2010**, *114*, 12305−12317.
(25) Mozhayskiy, V. A.; Krylov, A. I. ezSpectrum, http://iopenshell.usc.edu/downloads.
(26) Dunning, T. H. Gaussian-Basis Sets for Use in Correlated Molecular Calculations 0.1. The Atoms Boron through Neon and Hydrogen. *J. Chem. Phys.* **1989**, *90*, 1007−1023.
(27) Sinha, D.; Mukhopadhyay, S.; Mukherjee, D. A Note on the Direct Calculation of Excitation-Energies by Quasi-Degenerate MBPT and Coupled-ClusterTheory. *Chem. Phys. Lett.* **1986**, *129*, 369−374.
(28) Pal, S.; Rittby, M.; Bartlett, R. J.; Sinha, D.; Mukherjee, D. Multireference Coupled-Cluster Methods Using an Incomplete Model Space - Application to Ionization-Potentials and Excitation-Energies of Formaldehyde. *Chem. Phys. Lett.* **1987**, *137*, 273−278.
(29) Stanton, J. F.; Gauss, J. Analytic Energy Derivatives for Ionized States Described by the Equation-of-Motion Coupled-Cluster Method. *J. Chem. Phys.* **1994**, *101*, 8938−8944.
(30) Pieniazek, P. A.; Bradforth, S. E.; Krylov, A. I. Charge Localization and Jahn−Teller Distortions in the Benzene Dimer Cation. *J. Chem. Phys.* **2008**, *129*, 074104−074111.
(31) Krylov, A. I. Equation-of-Motion Coupled-Cluster Methods for Open-Shell and Electronically Excited Species: The Hitchhiker's Guide to Fock Space. *Annu. Rev. Phys. Chem.* **2008**, *59*, 433−462.
(32) Pieniazek, P. A.; Arnstein, S. A.; Bradforth, S. E.; Krylov, A. I.; Sherrill, C. D. Benchmark Full Configuration Interaction and Equation-of-Motion Coupled-Cluster Model with Single and Double Substitutions for Ionized Systems Results for Prototypical Charge Transfer Systems: Noncovalent Ionized Dimers. *J. Chem. Phys.* **2007**, *127*, 164110−164119.
(33) Becke, A. D. Density-Functional Exchange-Energy Approximation with Correct Asymtopic-Behavior. *Phys. Rev. A* **1988**, *38*, 3098−3100.
(34) Lee, C. T.; Yang, W. T.; Parr, R. G. Development of the Colle−Salvetti Correlation-Energy Formula into a Functional of the Electron-Density. *Phys. Rev. B* **1988**, *37*, 785−789.
(35) Shao, Y.; Molnar, L. F.; Jung, Y.; Kussmann, J.; Ochsenfeld, C.; Brown, S. T.; Gilbert, A. T. B.; Slipchenko, L. V.; Levchenko, S. V.; O'Neill, D. P.; et al. Advances in Methods and Algorithms in a Modern Quantum Chemistry Program Package. *Phys. Chem. Chem. Phys.* **2006**, *8*, 3172−3191.